Supporting Information for

Toward the Exact Exchange–Correlation Potential: A Three-Dimensional Convolutional Neural Network Construct

*Yi Zhou, Jiang Wu, Shuguang Chen, GuanHua Chen**

Department of Chemistry, The University of Hong Kong, Hong Kong S.A.R., China

AUTHOR INFORMATION

Corresponding Author

*Email: ghc@everest.hku.hk

I. Methods

A. CCSD and DFT calculation.

The CCSD calculation for H_2, HeH^+, He_2, linear H_3^+, and He–H–H–He^{2+} is carried out using the PySCF package.[1] The aug-cc-pVQZ basis set is used. Before calculating densities on real space grids, the outputted CCSD single-particle density matrices under molecular orbital basis set are transformed to density matrices under atomic orbital basis set. The KS-DFT calculation with the B3LYP functional used the same aug-cc-pVQZ basis set. A level 3 Lebedev-Laikov quadrature,[2] same as the one used in KS-DFT/NN SCF calculation, is used to evaluate the xc potential of B3LYP functional.

B. OEP procedure.

We employ the Wu-Yang method[3] to calculate the effective potential corresponding to the CCSD/aug-cc-pVQZ electron density. In the Wu-Yang method, the entire effective potential is expanded as:

$$v(\boldsymbol{r}) = v_{\text{ext}}(\boldsymbol{r}) + v_0(\boldsymbol{r}) + \sum_t b_t g_t(\boldsymbol{r}) \tag{S1}$$

where $v_{\text{ext}}(\boldsymbol{r})$ is the external potential due to the nuclei, $v_0(\boldsymbol{r})$ is fixed reference potential, and rest part of $v(\boldsymbol{r})$, denoted as $v_{\text{bg}}(\boldsymbol{r})$, is constructed by a linear combination of a set of Gaussian basis functions $\{g_t(\boldsymbol{r})\}$ with expansion coefficients $\{b_t\}$. The reference potential $v_0(\boldsymbol{r})$ we use consists of the Hartree term and the exchange term of the Hartree-Fock potential (HFX), which accounts for the major part of the KS effective potential, and ensures the correct $1/r$ asymptotic behavior for the xc potential. The same Gaussian type basis set for wave function calculation, aug-cc-pVQZ, is applied to the expansion of $v_{\text{bg}}(\boldsymbol{r}) = \sum_t b_t g_t(\boldsymbol{r})$. The optimization is carried out with a globally convergent Newton method,[4] and the truncated singular-value decomposition (TSVD) method with a cut-off of 5×10^{-6} (for H_2 and HeH^+) and 10^{-6} (for He_2) is used to finding the pseudo-inverse of the Hessian matrix. The CCSD densities and expanded potentials $v_{\text{bg}}(\boldsymbol{r})$ are used to construct the dataset for neural network.

C. Architecture of the 3D-CNN

To map the quasi-local electron density to the local xc potential, we employ a three-dimensional convolutional neural network (3D-CNN) as shown in **Figure S1**. The input or descriptors to the

3D-CNN are the quasi-local electron densities and their gradients centered at a spatial point $\boldsymbol{r}_i$ as depicted in **Figure 1a**; and the output is the value of the xc potential at $\boldsymbol{r}_i$, $v_{\mathrm{bg}}(\boldsymbol{r}_i)$. The grey cube is dissected into $9 \times 9 \times 9$ grids. The electron densities and their gradients along *x*-, *y*-, and *z*-directions form four $9 \times 9 \times 9$ tensors which are represented by the four cubes at the input layer of the 3D-CNN (see first column of **Figure S1**). $\boldsymbol{r}_i$ is chosen according to the Lebedev-Laikov quadrature. The coordinates of the grids in the cube are arranged as follows:

$$\left(x_p^i, y_q^i, z_r^i\right) = \left[x_0^i + (p-5)\,\mathrm{d}a, y_0^i + (q-5)\,\mathrm{d}a, z_0^i + (r-5)\,\mathrm{d}a\right] \qquad \text{(S2)}$$

where $p, q, r \in [1, 9]$ are the *x*, *y* and *z* indices of the grid, respectively. $\left(x_0^i, y_0^i, z_0^i\right) = \boldsymbol{r}_i$ is the centre of the cube, and da is the distance between two adjacent grids, equaling to 1/8 of the side length of the cube.

The four tensors at the input layer have in total 2916 elements, and are convoluted twice by two convolution kernels, leading to two convolutional layers, respectively. Each convolutional kernel is itself a tensor whose elements are determined through training. This is followed by a max-pooling procedure and resulted in a feature map which are represented by sixteen $2 \times 2 \times 2$ tensors. The feature map is then flattened into a vector of dimension 128, which is followed by three fully connected hidden layers of dimensions 64, 32 and 16, respectively. The final output is the value of the local xc potential at the center of the cube. The "exponential linear unit" (ELU)[5] activation function is applied to each convolutional layer and fully connected layer to provide non-linearity.

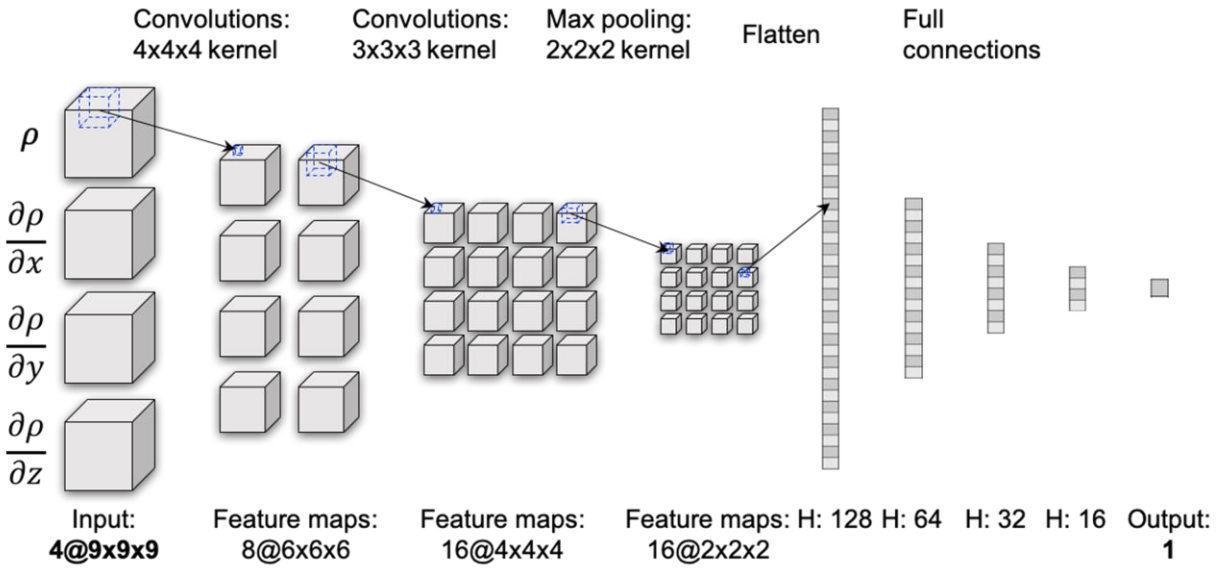

Figure S1. The architecture of three-dimensional convolutional neural network that maps the quasi-local density to local xc potential.

D. Training the 3D-CNN

The construction and training of neural network is carried out within PyTorch framework[6] on a NVIDIA GeForce GTX 1080 GPU. Minibatch stochastic gradient descent (SGD) with batch size of 200 data points is used during the training. The loss function of the 3D-CNN involves the mean-square-error (MSE) and a penalty function:

$$L = \frac{1}{N}\sum_{i=1}^{N}\left[\frac{\tilde{v}^{+}(\boldsymbol{r}_i) + \tilde{v}^{-}(\boldsymbol{r}_i)}{2} - v(\boldsymbol{r}_i)\right]^2 + [\tilde{v}^{+}(\boldsymbol{r}_i) - \tilde{v}^{-}(\boldsymbol{r}_i)]^2 \qquad \text{(S3)}$$

where $v(\boldsymbol{r}_i)$ is the target potential value on the quadrature point $\boldsymbol{r}_i$; the tilde values are the output from the 3D-CNN. The second term is the penalty term which ensures the invariance with respect to the index ordering of sampling points. For each quasi-local density sample $\rho_\Omega(\boldsymbol{r}_i)$ (denoted as $\rho_\Omega^{+}(\boldsymbol{r}_i)$), a correspondent sample $\rho_\Omega^{-}(\boldsymbol{r}_i)$ centered at the same quadrature point is generated with the coordinates of its sampling points re-arranged as:

$$\left(x_p^i, y_q^i, z_r^i\right) = \left[x_0^i + (p-5)\,\mathrm{d}a, y_0^i + (q-5)\,\mathrm{d}a, z_0^i - (r-5)\,\mathrm{d}a\right] \qquad \text{(S4)}$$

The corresponding predictions of the two inputs, $\tilde{v}^{+}(\boldsymbol{r}_i)$ and $\tilde{v}^{-}(\boldsymbol{r}_i)$, are averaged to compute the MSE loss, *i.e.*, the first term of Eq. (S4), and their difference leads to the non-negative penalty term. During the training process, the penalty term is minimized along with the total loss function. The invariant of the 3D-CNN with respect to the ordering of the sampling points along z-direction

in the input is thus ensured. Similar terms can be added to ensure that the mapping $\rho_\Omega(\boldsymbol{r}_i) \rightarrow v(\boldsymbol{r}_i)$ is invariant with respect to symmetry operations on the quasi-local density inputs.

II. Detailed *I* values and electron density differences compared to the CCSD benchmarks

A. H2/HeH+ system

To investigate the consistency of electron densities obtained via the KS-DFT/NN calculation, we performed a series of SCF calculations using different initial values. The convergent electron densities are compared to each other and to the CCSD benchmark using the *I* values. Typical results of $I_{\text{NN-X,NN-Y}}$ and $I_{\text{NN-X,CCSD}}$ (where X and Y denotes the method to get initial value for KS-DFT/NN SCF calculation and can be LDA, PBE, B3LYP, and CCSD) for equilibrium H_2 and HeH^+ structure are summarized in **Table S1**. The extreme small $I_{\text{NN-X,NN-Y}}$ values around 10^{-16} confirm the consistency of convergent density distribution starting from different initial values, indicating that the KS-DFT/NN SCF calculation can start with less computationally intensive functionals (*e.g.*, LDA) as the initial guess.

Table S1. *I* values between KS-DFT/NN densities using different initial values and the CCSD benchmarks for equilibrium H_2 and HeH^+

Mol.	Method	NN-LDA	NN-PBE	NN-B3LYP	NN-CCSD*	CCSD
H_2	NN-LDA	0	3.531×10^{-16}	1.363×10^{-16}	9.242×10^{-16}	2.344×10^{-7}
	NN-PBE	3.531×10^{-16}	0	7.549×10^{-17}	1.374×10^{-16}	2.344×10^{-7}
	NN-B3LYP	1.363×10^{-16}	7.549×10^{-17}	0	3.933×10^{-16}	2.344×10^{-7}
	NN-CCSD*	9.242×10^{-16}	1.374×10^{-16}	3.933×10^{-16}	0	2.344×10^{-7}
	CCSD	2.344×10^{-7}	2.344×10^{-7}	2.344×10^{-7}	2.344×10^{-7}	0
HeH^+	NN-LDA	0	2.682×10^{-17}	6.700×10^{-17}	1.652×10^{-17}	4.114×10^{-7}
	NN-PBE	2.682×10^{-17}	0	2.199×10^{-17}	3.945×10^{-17}	4.114×10^{-7}
	NN-B3LYP	6.700×10^{-17}	2.199×10^{-17}	0	7.155×10^{-17}	4.114×10^{-7}
	NN-CCSD*	1.652×10^{-17}	3.945×10^{-17}	7.155×10^{-17}	0	4.114×10^{-7}
	CCSD	4.114×10^{-7}	4.114×10^{-7}	4.114×10^{-7}	4.114×10^{-7}	0

* Using CCSD density as initial guess is for comparison purpose only.

Typical $I_{B3LYP,CCSD}$ and $I_{NN,CCSD}$ values of 201 H_2 and HeH^+ structures with internuclear distance ranging from 0.5 Å to 0.9 Å are summarized in **Table S2**. The $I_{NN,CCSD}$ are approximately one order of magnitude smaller than $I_{B3LYP,CCSD}$ for test structures.

Table S2. Selected *I* values between density and the CCSD benchmarks ($\times 10^{-5}$) for H_2 and HeH^+

Mol.	Method	0.500 Å	0.600 Å	0.700 Å	0.800 Å	0.900 Å	Equilibrium*
H_2	B3LYP	4.524	5.284	6.037	6.547	6.646	6.294
	KS-DFT/NN	0.233	0.115	0.013	0.232	1.747	0.023
HeH^+	B3LYP	3.473	4.255	4.850	5.259	5.528	5.170
	KS-DFT/NN	0.162	0.008	0.016	0.056	0.153	0.041

*Equilibrium distance determined from CCSD calculation: H_2 0.7420 Å and HeH^+ 0.7748 Å

B. Van der Waals interaction: He_2 from H_2/HeH^+ system

The 3D-CNN model trained with H_2/HeH^+ dataset is applied to the He_2 molecule. Typical $I_{B3LYP,CCSD}$ and $I_{NN,CCSD}$ values of He_2 structures with internuclear distance ranging from 2.0 Å to 3.2 Å is summarized in **Table S3**. The $I_{NN,CCSD}$ are smaller than $I_{B3LYP,CCSD}$, but the improvement is not as significant, indicating that current 3D-CNN can recognize only partial vdW interaction from the H_2/HeH^+ dataset. More comprehensive dataset and training process will be required to further improve the accuracy of He_2 densities.

Table S3. Selected *I* values compared to the CCSD benchmarks for He_2 using H_2/HeH^+ dataset

Mol.	Method	2.00 Å	2.40 Å	2.80 Å	3.20 Å	Equilibrium*
He_2	B3LYP ($\times 10^{-5}$)	4.522	4.527	4.520	4.514	4.516
	KS-DFT/NN ($\times 10^{-5}$)	1.541	1.233	1.139	1.116	1.123

* Equilibrium distance determined from CCSD calculation: He_2 3.01 Å

C. Transferability: linear H_3^+ structures

Currently, our approach can only deal with linear systems. The density difference compared to the CCSD benchmark is plotted in **Figure S2**. Representative results of H_3^+ structures with shortest (0.6 Å), medium (0.7 Å) and longest (0.8 Å) H–H distance show clearly that the electron density obtained via KS-DFT/NN calculation is more accurate than B3LYP results, especially at nuclear

sites.. The I values of all 441 structures are exhibits in **Figure S3**. The average I value is 8.53×10^{-5} for $I_{\mathrm{B3LYP,CCSD}}$ and 4.67×10^{-5} for $I_{\mathrm{NN,CCSD}}$.

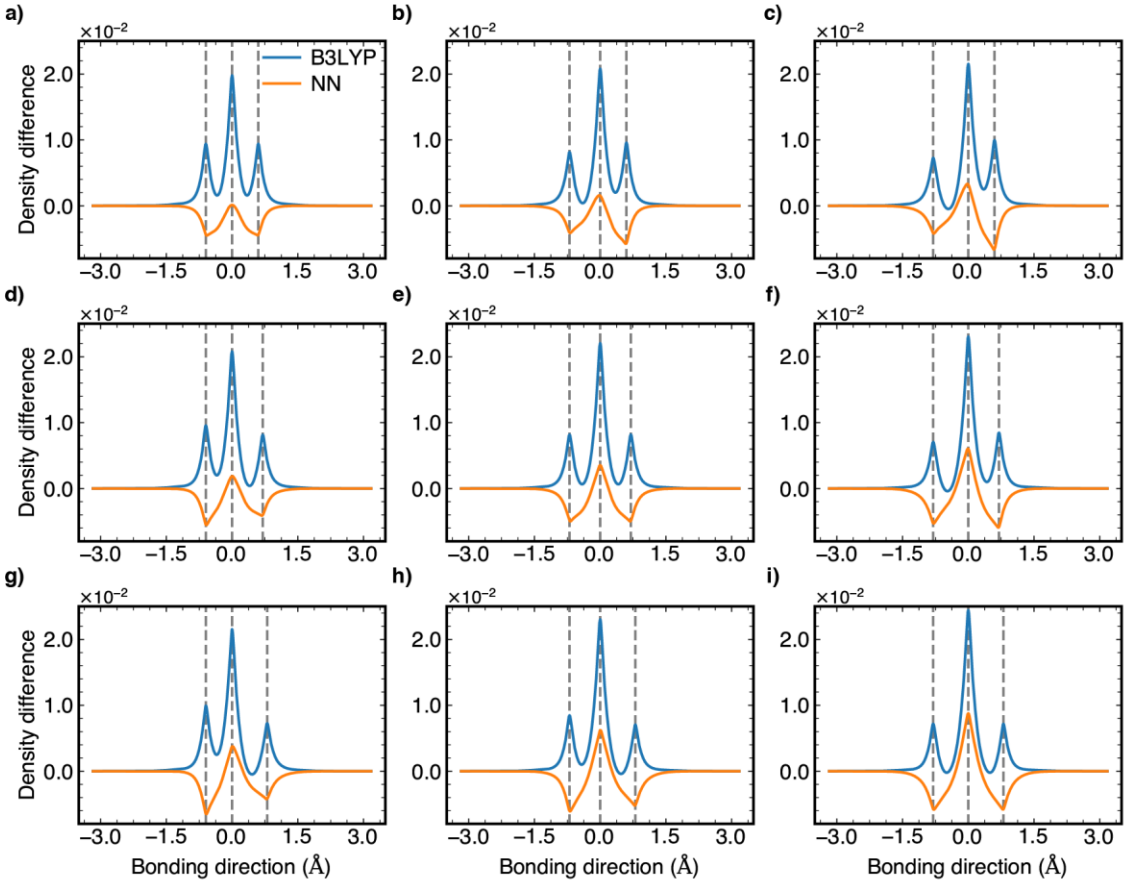

Figure S2. Differences between calculated densities and the CCSD benchmarks for a variety of linear H–H–H^+ structures along the internuclear direction using H_2/HeH^+ dataset. The right and left H–H distances are (a) 0.60 Å, 0.60 Å; (b) 0.60 Å, 0.70 Å; (c) 0.60 Å, 0.80 Å; (d) 0.70 Å, 0.60 Å; (e) 0.70 Å, 0.70 Å; (f) 0.70 Å, 0.80 Å; (g) 0.80 Å, 0.60 Å; (h) 0.80 Å, 0.70 Å; (i) 0.80 Å, 0.80 Å.

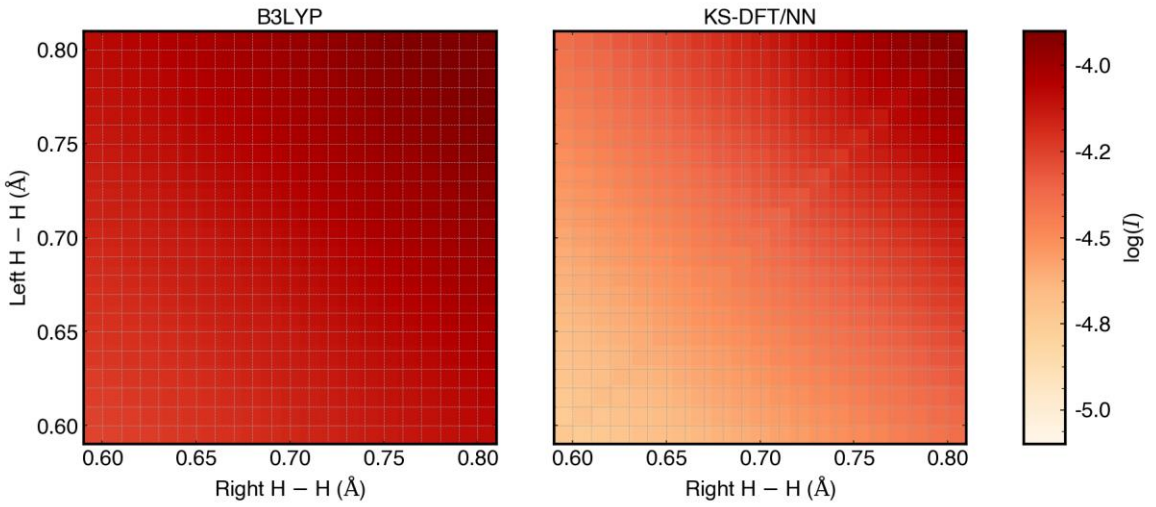

Figure S3. Normalized squared differences compared to the CCSD benchmark for 441 linear H_3^+ structures using H_2/HeH^+ dataset. Left part shows $I_{B3LYP,CCSD}$ computed using B3LYP electron densities. Right part shows $I_{NN,CCSD}$ computed using electron densities from KS-DFT/NN calculation.

D. Transferability: He–H–H–He^{2+} structures

The density difference compared to the CCSD benchmark is plotted in **Figure S4**. We choose only symmetric structures (*i.e.*, two He–H distances are identical). Representative results of He–H–H–He^{2+} structures with shortest (0.6 Å), medium (0.7 Å) and longest (0.8 Å) H–H and He–H distance show clearly that the electron density obtained via KS-DFT/NN calculation is more accurate than B3LYP results, especially at nuclear sites. The I values of all 441 structures are exhibits in **Figure S5**. The average value is 8.00×10^{-5} for $I_{B3LYP,CCSD}$ and 1.57×10^{-5} for $I_{NN,CCSD}$.

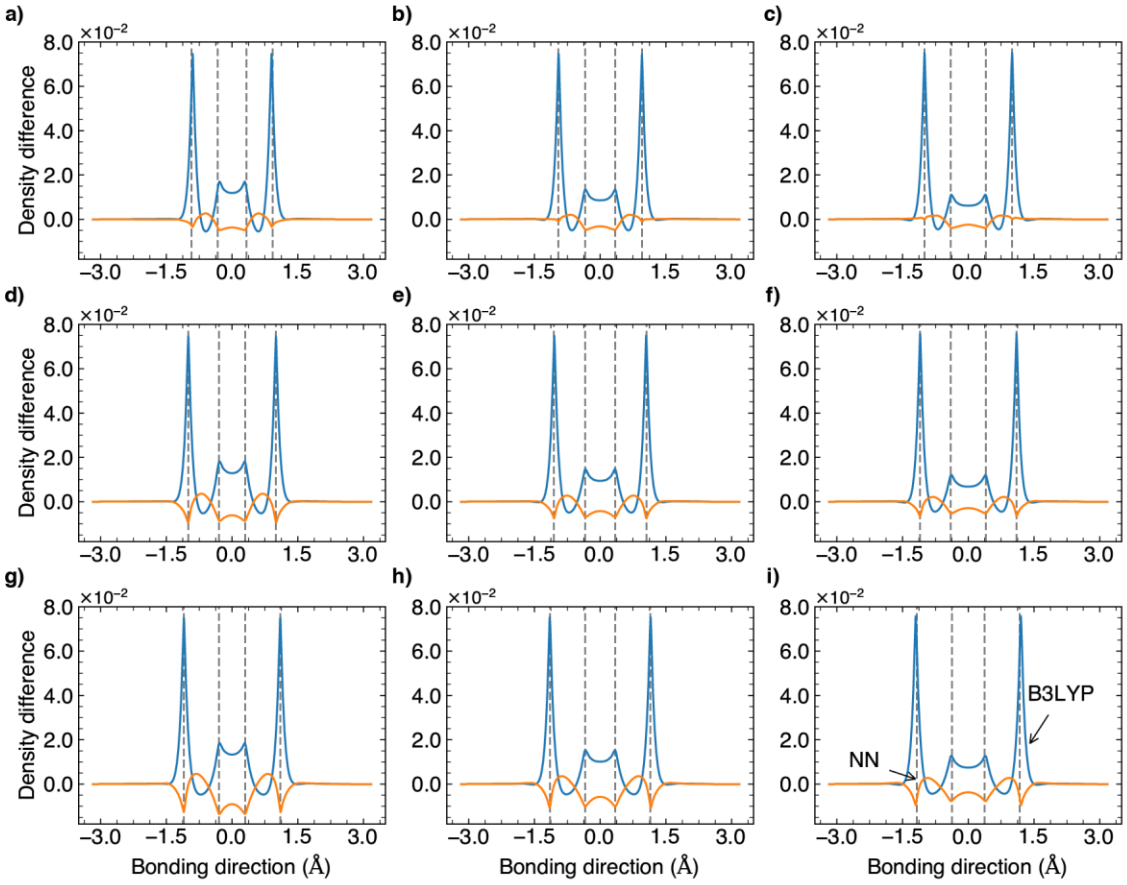

Figure S4. Differences between calculated densities and the CCSD benchmarks for a variety of He–H–H–He^{2+} structures along the internuclear direction using H_2/HeH^+ dataset. The He–H and H–H distances are (a) 0.60 Å, 0.60 Å; (b) 0.60 Å, 0.70 Å; (c) 0.60 Å, 0.80 Å; (d) 0.70 Å, 0.60 Å; (e) 0.70 Å, 0.70 Å; (f) 0.70 Å, 0.80 Å; (g) 0.80 Å, 0.60 Å; (h) 0.80 Å, 0.70 Å; (i) 0.80 Å, 0.80 Å.

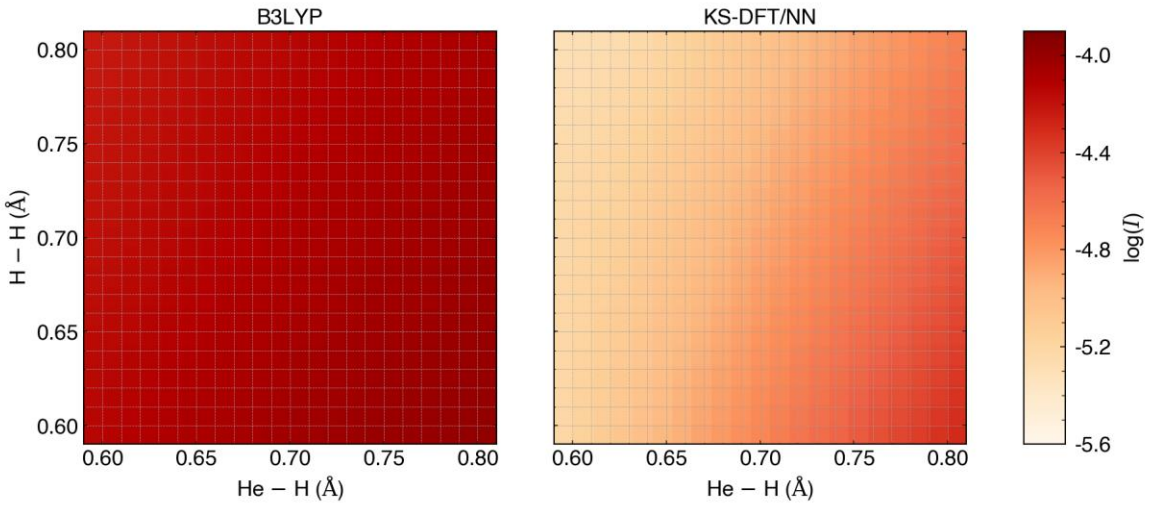

Figure S5. Normalized squared differences compared to the CCSD benchmark for 441 He–H–H–He^{2+} structures using H_2/HeH^+ dataset. Left part shows $I_{B3LYP,CCSD}$ computed using B3LYP electron densities. Right part shows $I_{NN,CCSD}$ computed using electron densities from KS-DFT/NN calculation.

E. Van der Waals interaction: He_2 system

Typical $I_{B3LYP,CCSD}$ and $I_{NN,CCSD}$ values of 61 He_2 structures with internuclear distance ranging from 2.0 Å to 3.2 Å is summarized in **Table S4**. The $I_{NN,CCSD}$ are more than three orders of magnitude smaller than $I_{B3LYP,CCSD}$.

Table S4. Selected *I* values between density and the CCSD benchmarks for He_2

Mol.	Method	2.00 Å	2.40 Å	2.80 Å	3.20 Å	Equilibrium*
He_2	B3LYP ($\times10^{-5}$)	4.522	4.527	4.520	4.514	4.516
	KS-DFT/NN ($\times10^{-8}$)	3.757	0.545	0.574	0.695	0.641

* Equilibrium distance determined from CCSD calculation: He_2 3.01 Å

F. H_2/HeH^+/He_2 system

Representative results of density difference of symmetric He–H–H–He^{2+} structures compared to the CCSD benchmark is plotted in **Figure S6**. Similar to the H_2/HeH^+ cases, **Figure S6** shows clearly that the electron density obtained via KS-DFT/NN calculation is more accurate than

B3LYP results, especially at nuclear sites.. The I values of all 441 structures are exhibited in **Figure S7**. The average I value is 8.00×10^{-5} for $I_{\mathrm{B3LYP,CCSD}}$ and 1.86×10^{-5} for $I_{\mathrm{NN,CCSD}}$.

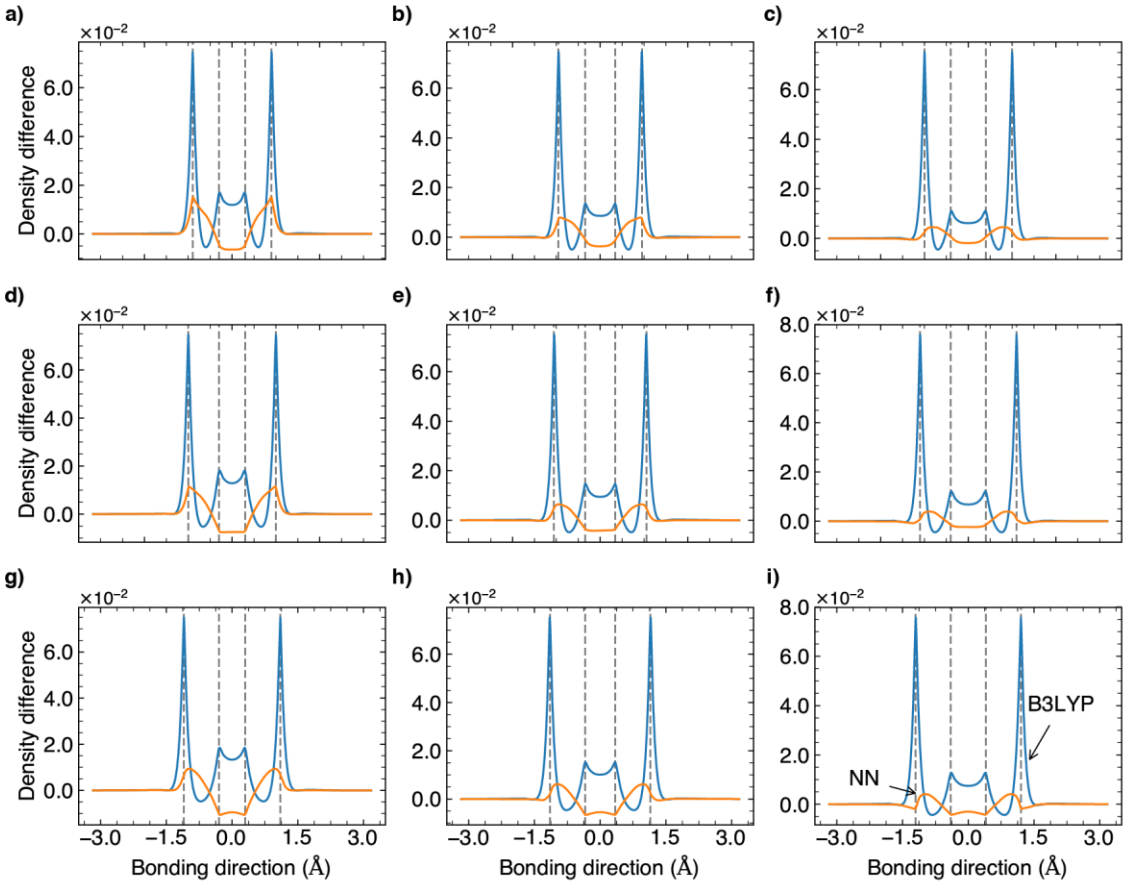

Figure S6. Differences between calculated densities and the CCSD benchmarks for a variety of He–H–H–He^{2+} structures along the internuclear direction using H_2/HeH^+/He_2 dataset. The He–H and H–H distances are (a) 0.60 Å, 0.60 Å; (b) 0.60 Å, 0.70 Å; (c) 0.60 Å, 0.80 Å; (d) 0.70 Å, 0.60 Å; (e) 0.70 Å, 0.70 Å; (f) 0.70 Å, 0.80 Å; (g) 0.80 Å, 0.60 Å; (h) 0.80 Å, 0.70 Å; (i) 0.80 Å, 0.80 Å.

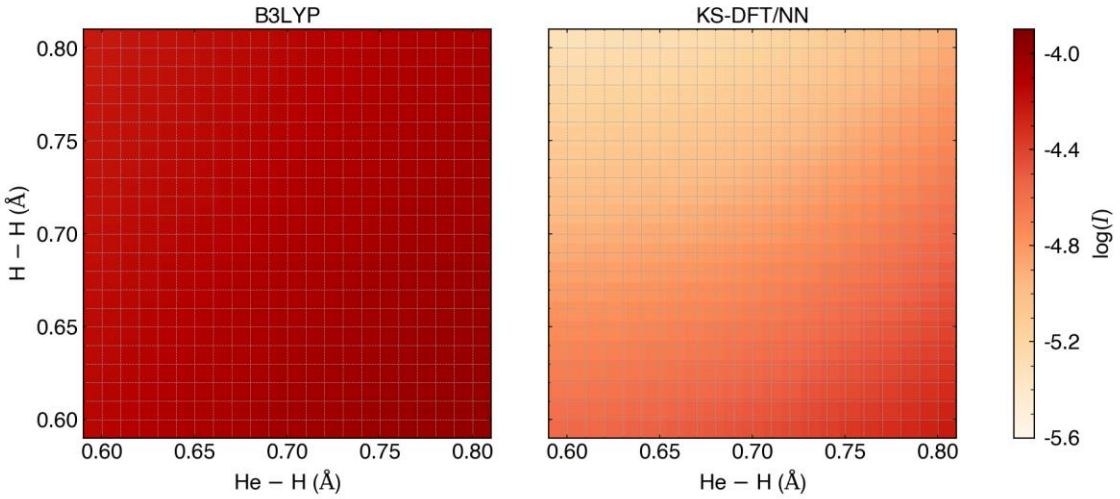

Figure S7. Normalized squared differences compared to the CCSD benchmark for 441 He–H–H–He^{2+} structures using H_2/HeH^+/He_2 dataset. Left part shows $I_{B3LYP,CCSD}$ computed using B3LYP electron densities. Right part shows $I_{NN,CCSD}$ computed using electron densities from KS-DFT/NN calculation.

Reference

1. Sun, Q.; Berkelbach, T. C.; Blunt, N. S.; Booth, G. H.; Guo, S.; Li, Z.; Liu, J.; McClain, J. D.; Sayfutyarova, E. R.; Sharma, S.; Wouters, S.; Chan, G. K.-L. PySCF: the Python-Based Simulations of Chemistry Framework. *Wiley Inter. Rev. Comput. Mol. Sci.* **2017,** *8*, e1340.

2. Lebedev, V. I.; Laikov, D. N. A Quadrature Formula for the Sphere of the 131st Algebraic Order of Accuracy, *Dokl. Math.* **1999,** *59*, 477-481.

3. Wu, Q.; Yang, W. A Direct Optimization Method for Calculating Density Functionals and Exchange–Correlation Potentials from Electron Densities. *J. Chem. Phys.* **2003,** *118*, 2498-2509.

4. Press, W. H.; Teukolsky, S. A.; Vetterling, W. T.; Flannery, B. P. *Numerical Recipes in C: The Art of Scientific Computing (2nd Ed.)*. Cambridge University Press: New York, USA; 1992.

5. Clevert, D.-A.; Unterthiner, T.; Hochreiter, S. Fast and Accurate Deep Network Learning by Exponential Linear Units (ELUs). In *International Conference on Learning Representations*, San Juan, Puerto Rico, May 2–4, 2016; arXiv:1511.07289 https://arxiv.org/pdf/1511.07289.

6. Paszke, A.; Gross, S.; Chintala, S.; Chanan, G.; Yang, E.; DeVito, Z.; Lin, Z.; Desmaison, A.; Antiga, L.; Lerer, A. Automatic differentiation in PyTorch, In *NIPS 2017 Workshop Autodiff*, Long Beach, CA, USA December 9, 2017; https://openreview.net/pdf?id=BJJsrmfCZ.